CFD SIMULATIONS OF LID DRIVEN CAVITY FLOW AT MODERATE REYNOLDS NUMBER

Reyad Omari

Department of Mathematics, Al-Balqa Applied University,

Irbid University college, Irbid, Jordan

Abstract

Computational fluid dynamics (CFD) simulations are carried out for laminar incompressible fluid flow in lid driven cavity ($10 \leq Re \leq 1000$). The ratio of the height to the width of the cavity are ranged over $H/L = 0.5$ to 1.5. A commercial finite volume package FLUENT was used to analyze and visualize the nature of the flow inside the cavity of different aspect ratio. The simulation results are presented in terms of velocity profile, pressure coefficient and stream contours. It was found that the pressure coefficient inside the cavity is strongly governed by the aspect ratio as well as the Reynolds number. Velocity profile for special case of a square cavity ($AR = 1$) was found to be in good agreement with previous experimental results. The present study has established that commercially-available software like FLUENT can provide a reasonable good solution of complicated flow structures including flow inside cavities.

Keywords: CFD simulation, Laminar flow, Drag coefficient, Lid driven cavity

Introduction

The lid-driven cavity flow is the motion of a fluid inside a rectangular cavity created by a constant translational velocity of one side while the other sides remain at rest. Fluid flow behaviors inside lid driven cavities have been the subject of extensive computational and experimental studies over the past years. Applications of lid driven cavities are in material processing, dynamics of lakes, metal casting and galvanizing.

The macroscopic variables of interest in conventional numerical methods, such as velocity and pressure are usually obtained by solving the Navier-Stokes equation. Such numerical methods for two dimensional steady incompressible Navier-Stokes equations are often tested for code validation. The one sided lid-driven square cavity flow has been used as

a benchmark problem for many numerical methods due to its simple geometry and complicated flow behaviors. It is usually very difficult to capture the flow phenomena near the singular points at the corners of the cavity (Chen, 2009 and 2011. Migeon et al. (2003)

(N. A. C. Sidik and S. M. R. Attarzadeh, 2011) considered the cubic interpolated pseudo particle method and validate their results with the shear driven flow in shallow cavities. (Li et al., 2011) applied the new version of multiple relaxation time lattices Boltzmann method to investigate the fluid flow in deep cavity.

There have been some works devoted to the issue of heat transfer in the shear driven cavity. (Manca et al., 2003) presented a numerical analysis of laminar mixed convection in an open cavity with a heated wall bounded by a horizontally insulated plate. Results were reported for Reynolds numbers from 100 to 1000 and aspect ratio in the ranges from 0.1 to 1.5. They presented that the maximum decrease in temperature was occurred at higher Reynolds. The effect of the ratio of channel height to the cavity height was found to be played a significant role on streamlines and isotherm patterns for different heating configurations. The investigation also indicates that opposing forced flow configuration has the highest thermal performance, in terms of both maximum temperature and average Nusselt number.

(Gau and Sharif, 2004) reported mixed convection in rectangular cavities at various aspect ratios with moving isothermal side walls and constant flux heat source on the bottom wall. Numerical simulation of unsteady mixed convection in a driven cavity using an externally excited sliding lid is conducted by (Khanafer et al. 2007). They observed that, *Re* and *Gr* would either enhance or retard the energy transport process and drag force behavior depending on the conduct of the velocity cycle.

(Ch.-H. Bruneau and M. Saad, 2006, Batchelor, (1956), have pointed out that, driven cavity flows exhibit almost all the phenomena that can possibly occur in incompressible flows: eddies, secondary flows, complex three-dimensional patterns, chaotic particle motions, instability, and turbulence. Thus, these broad spectra of features make the cavity flows overwhelmingly attractive for examining the computational schemes.

This paper aims to provide a CFD simulation study of incompressible viscous laminar flow in cavity flow over arrange of aspect ratio ($0.5 \leq AR \leq 1.5$) by using commercial finite volume package FLUENT. Another sub goal of the present study is to test whether FLUENT, a commercial Computational Fluid Dynamics (CFD) software package, is capable of providing the solutions for the problem under consideration.

Theoretical Formulation

Governing equations

The fluid flow in open lid driven cavity can be simulated by a set of mass and momentum conservation equations. The flow is assumed to be two-dimensional, laminar, incompressible and Newtonian. The governing non-linear partial differential equations can be written as follows:

continuity equation:

$$\frac{\partial U}{\partial X}+\frac{\partial V}{\partial Y}=0 \tag{1}$$

x-momentum equation:

$$\frac{\partial U}{\partial \tau}+U\frac{\partial U}{\partial X}+V\frac{\partial U}{\partial Y}=-\frac{\partial P}{\partial Y}+\frac{1}{Re}\left[\frac{\partial^2 U}{\partial X^2}+\frac{\partial^2 U}{\partial X^2}\right] \tag{2}$$

y-momentum equation:

$$\frac{\partial V}{\partial \tau}+U\frac{\partial V}{\partial X}+V\frac{\partial V}{\partial Y}=-\frac{\partial P}{\partial Y}+\frac{1}{Re}\left[\frac{\partial^2 V}{\partial X^2}+\frac{\partial^2 V}{\partial X^2}\right] \tag{3}$$

The above equations were non-dimensionalized as follows:

$$U=\frac{u}{U_\infty}\ ; \qquad V=\frac{v}{U_\infty}\ ; \qquad X=\frac{x}{L}; \qquad Y=\frac{y}{L}; \tag{4}$$

and

$$\tau=\frac{tU_\infty}{L}; \qquad P=\frac{p}{\rho U_\infty}; \qquad Re=\frac{U_\infty l}{\nu}; \tag{5}$$

The L is the reference length dimension (width of the cavity along lower lid), while U_∞ is the reference velocity dimension. The fluid property ν, refers to the kinematic viscosity. The Reynold's number, *Re,* is the ratio of inertial to viscous forces, which influences the fluid flow features within the cavity.

Boundary conditions

No-slip velocity boundary condition (u = v = 0) is applied on all the walls, except the top lid. On the top lid (U= 1 and V = 0) is applied. The bottom boundary of the domain is modeled as wall .The boundary conditions which describing the current simulated computational domain as well as the surface boundary layer is depicted in Figure 1.

Numerical Methods

A finite volume method is employed using commercial software FLUENT 6.2 to solve the governing equations subject to specified boundary conditions. Since the boundary layer separation is intimately connected with the pressure and velocity distribution in the

boundary layer, accurate separation point predication are dependent on accurate resolution of the boundary layer near the surface of the cavity. More cells are constructed near the surface of the cavity to compensate the high velocity gradient in the boundary layer region of the viscous flow. A commercial software GAMBIT is used for grid generation. The coupling between the pressure and velocity fields is achieved using PISO. A second order upwind scheme is used for the convection. Here in this study, following [10], we define the pressure drag coefficient, C_P as follows:

$$C_p = \frac{2(p - p_\infty)}{\rho U_\infty^2 A} \tag{6}$$

p_∞ is the pressure of the stream, *A* is appropriate cavity surface area and U_∞ is lid velocity. The grid independence is achieved by comparing the results of the different grid cell size. It was found that 65000 cells are satisfactory, and any increase beyond this size would lead to an insignificant change in the resulting solution.

Results and Discussion

Simulation results for incompressible laminar flow in square cavity (*AR* = 1) are compared to experimental data to verify the validity of the CFD simulation solution. Fig. 2 and Fig. 3 show the U and V-velocity profiles along a vertical and horizontal line respectively passing through the geometric centre of the square cavity for (AR = 1). As can be seen there is an excellent agreement in the velocity profile between CFD simulations in this study and the experimental measured by.

First, the influence of the cavity aspect ratio on the flow field in the cavity is shown in Fig. 4 and 5 while the Reynolds number was fixed. Fig. 4 and 5 demonstrate the computed U-velocity along a vertical line passing through the geometric centre of the different aspect ratio cavity for Re = 1000 and 100 respectively. It is clear that the core of the vortices lay near the vicinity of the corner of the cavity for large aspect ratio. In addition, one may notice that as Reynolds number increases thin boundary layers are developed along the solid walls and the core fluid moves as a solid body with a uniform vorticity, in the manner suggested by [3]. Fig. 6 and 7 demonstrate the computed V-velocity along a horizontal line passing through the geometric centre of the square cavity for Re = 1000 and 100 respectively. They show a gradually decreasing velocity near the centre and the development of narrow boundary layers along the walls regardless the aspect ratio. For low Reynolds number a thicker boundary layer is produced. It can be also noted that the boundary layer produced for low aspect ratio is thinner along the walls. In both figures the changes in the velocity direction lead to vortex development.

Fig. 8, 9 and 10 demonstrate the computed U- velocity along a vertical line passing through the geometric centre of the different aspect ratio cavity for Re = 1000, 500 and 100 respectively. As might be expected, near the lid the stream wise U-component displays a steadily thinner boundary layer as *Re* increased regardless the aspect ratio. But at the bottom wall, counterintuitively, the peak U decreases with Reynolds number although it does move towards the wall as expected. For AR = 0.5 the effect of Rynolds number on the U-velocity is insignificant and dominant for large aspect ratio.

The dimensionless pressure drop coefficient for the cavity is an important parameter in the design of the cavity. In Fig. 11 the variation of the pressure drop coefficient along a vertical line passing through the geometric centre of the different aspect ratio cavity is shown. The pressure drop coefficient is a strong function of the position, aspect ratio and Reynolds number. It can be noted that the pressure drop coefficient is higher for lower aspect ratio. The pressure drop coefficient attains its maximum value within the above half cavity, whereas for most cavity aspect ratio it gains the minimum value with the bottom half cavity.

In order to visualize the overall flow patterns, the streamline plots from the computational data for different aspect ratio are at different Reynolds number is shown in Fig. 11 and Fig.12. For smaller aspect ratio the center of the primary eddy moves right with respect to right wall cavity. However, as the aspect ratio increases beyond a value of 1, the center of the primary eddy remain constant below the top lid for Reynolds number 100. At high value of Reynolds number, strong shear force drags the flow and causes the vortex to break into two smaller vortices for AR= 0.5 and AR =1.5. For aspect ratio AR = 1.0 and high Reynolds number the primary eddy shifted to the center of the cavity (see Fig.12).

Conclusion

Computational fluid dynamics (CFD) simulations are carried out for laminar incompressible fluid flow in lid driven cavity fordifferent aspect ratio. The nature of the flow inside lid driven cavity of different aspect ratio was visualized. It was found that the dynamics and structure of primary vortex are strongly affected by the Reynolds number as well as the aspect ratio of the cavity. It was noted that the pressure drop coefficient is a strong function of the position, aspect ratio and Reynolds number. Comparison the simulation results with the experimental data validate the commercially-available software FLUENT in providing a reasonable good solution of complicated flow structures, including flow with separation.

References:

(Chen S 2009) A large-eddy-based lattice Boltzmann model for turbulent flow simulation. Applied Mathematics and Computation, 215, 591–595.

N. A. C. Sidik and S. M. R. Attarzadeh, An accurate numerical prediction of solid particle fluid flow in a lid-driven cavity. Intl. J. Mech. 2011, 5(3): 123-128.

S.L. Li, Y.C. Chen, and C.A. Lin. Multi relaxation time lattice Boltzmann simulations of deep lid driven cavity flows at different aspect ratios. Comput. & Fluids, 2011, 45(1): 233-240.

A.J. Chamkha, Hydromagnetic combined convection flow in a vertical lid-driven cavity with internal heat generation or absorption, *Numer. Heat Transfer, Part A*, vol. 41, pp.529-546, 2002.

K.M. Khanafer, A.M. Al-Amiri and I. Pop, Numerical simulation of unsteady mixed convection in a driven cavity using an externally excited sliding lid, *European J. Mechanics B/Fluids*, vol. 26, pp.669-687, 2007.

G.K. Batchelor. On Steady Laminar Flow with Closed Streamlines at Large Reynolds Numbers. *J. Fluid Mech.* 1956; **1**:177–190.

O. Manca, S. Nardini, K. Khanafer and K. Vafai, Effect of Heated Wall Position on Mixed Convection in a Channel with an Open Cavity, *Numer. Heat Transfer, Part A*, vol. 43, pp.259–282, 2003.

G. Gau and M.A.R. Sharif, Mixed convection in rectangular cavities at various aspect ratios with moving isothermal side walls and constant flux heat source on the bottom wall *Int. J. Therm. Sci.*, **43**, pp. 465–475, 2004.

C. Migeon, G. Pineau, and A. Texier, Three-dimensionality development inside standard parallel pipe lid-driven cavities at Re = 1000. J. Fluids and Struc. 2003, 17 (1): 717–738.

Ch.-H. Bruneau, M. Saad, The 2D lid-driven cavity problem revisited, Computers & Fluids35 (3), 2006.

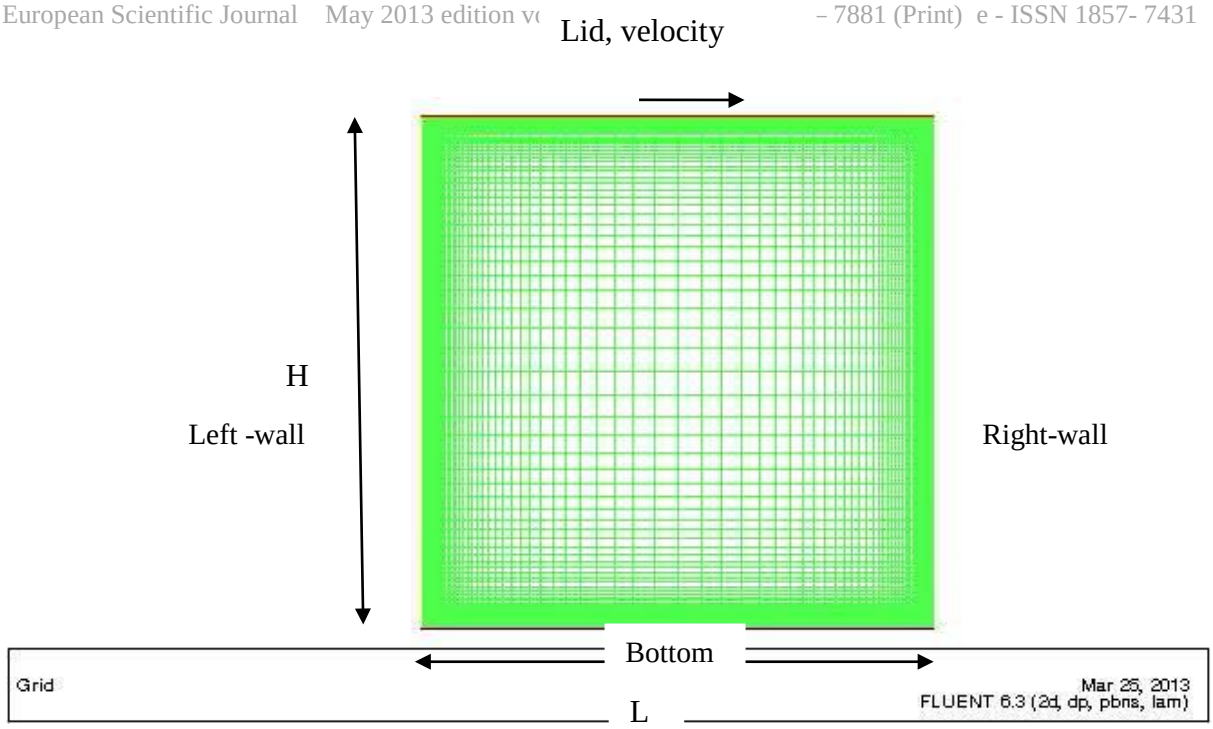

Figure 1: Computational mesh for the lid-driven square cavity, AR = 1 (65000 cells)

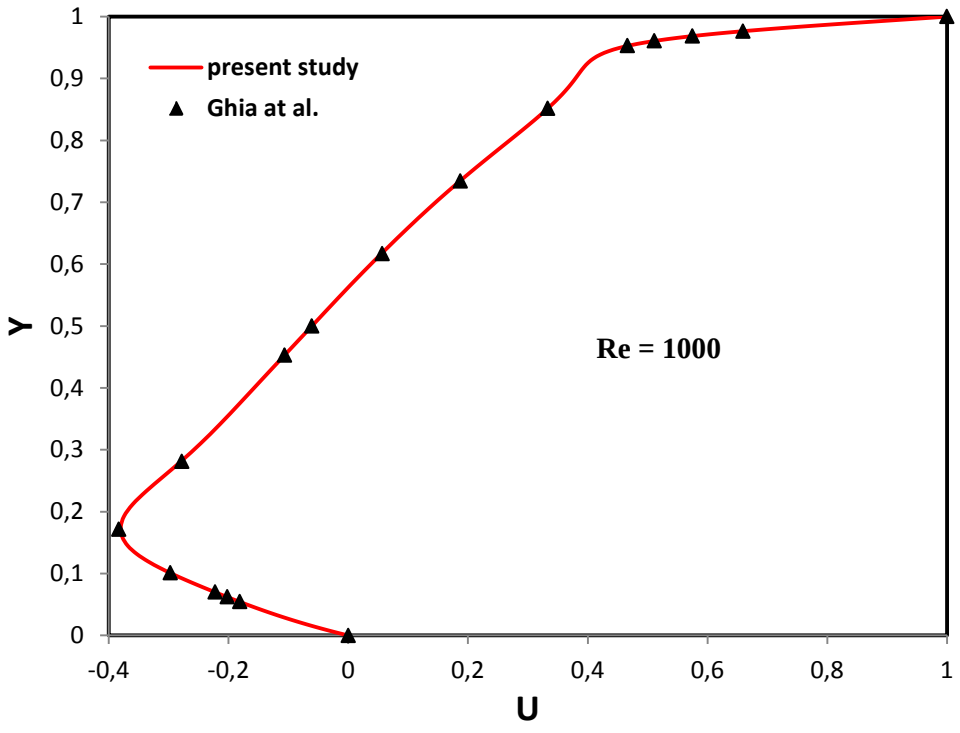

Figure 2: Comparison of U-velocity profiles along a vertical line passing through the geometric centre of the cavity (at X= 0.5)

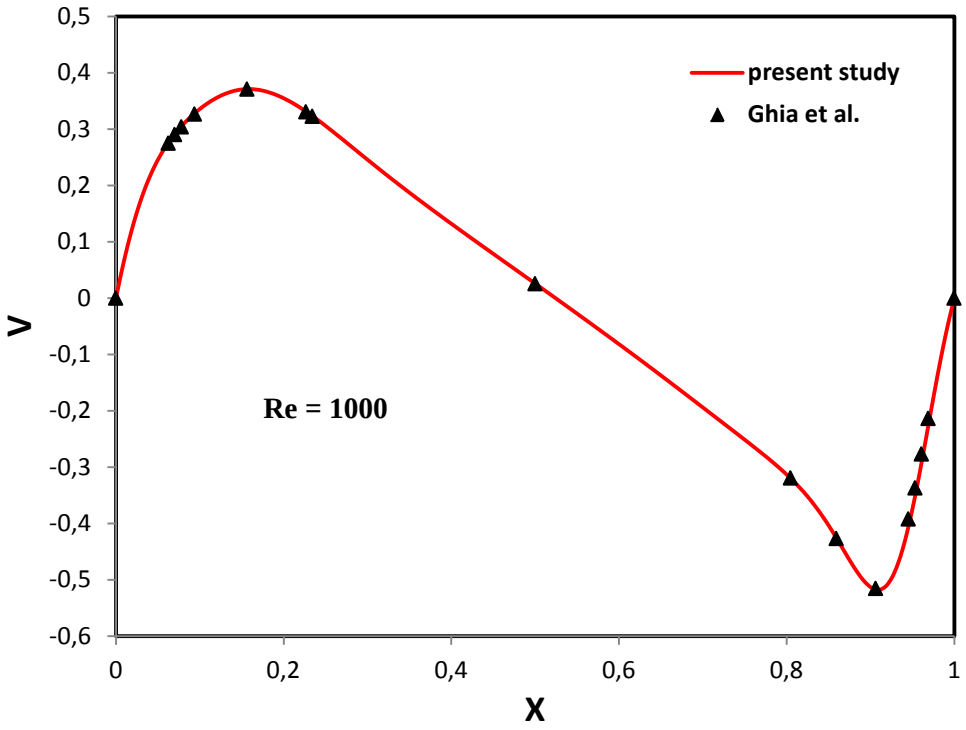

Figure 3: Comparison of V-velocity profiles along a horizontal line passing through the geometric centre of the cavity (at Y= 0.5)

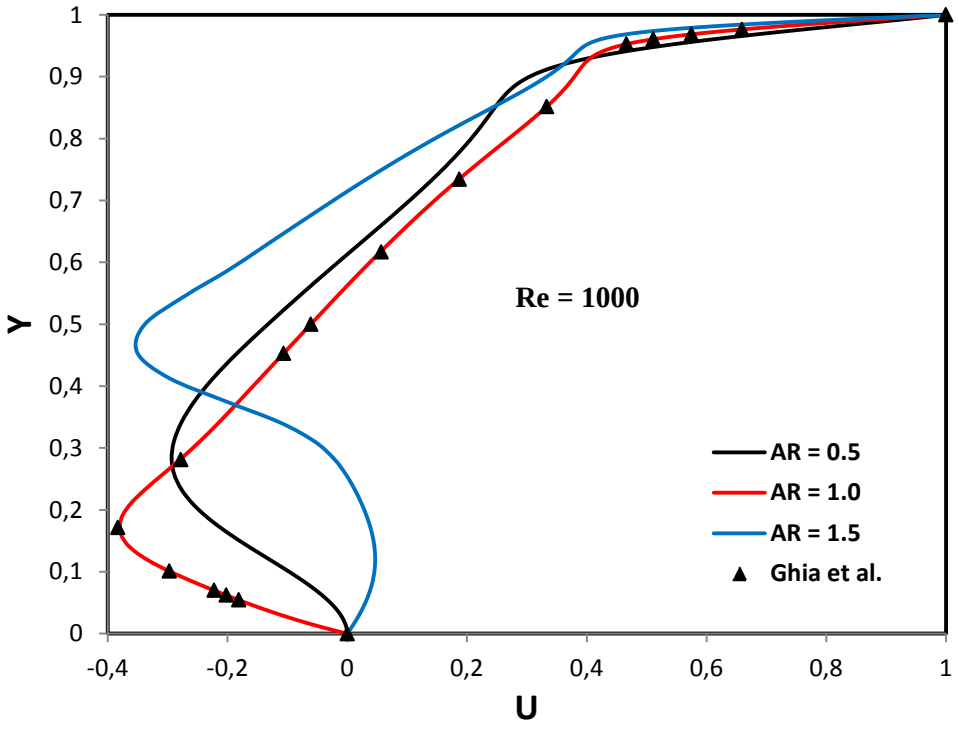

Figure 4: Computed of U-velocity profiles along a vertical line passing through the geometric centre of the cavity (at X= 0.5) at various aspect ratios, Re = 1000.

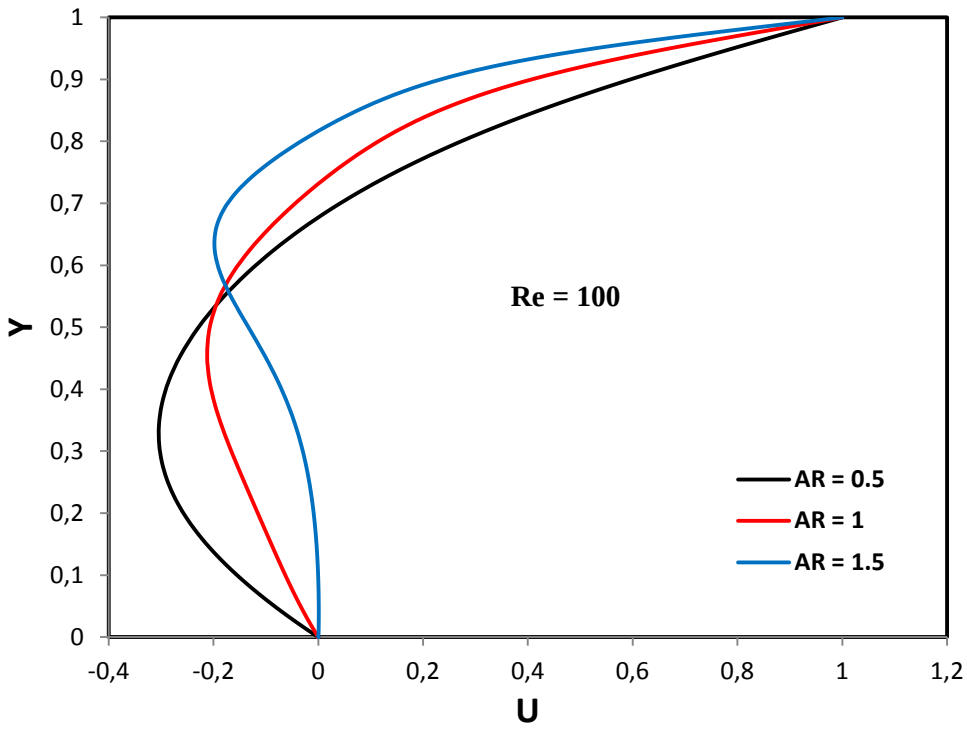

Figure 5: Computed of U-velocity profiles along a vertical line passing through the geometric centre of the cavity (at X= 0.5) at various aspect ratios, Re = 100.

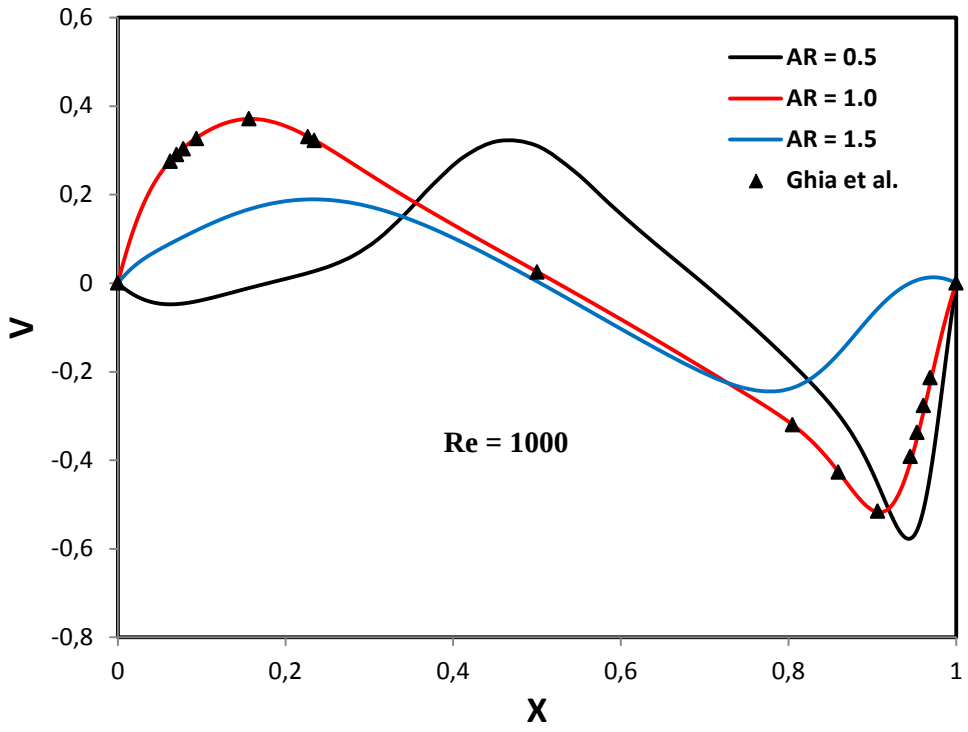

Figure 6: Computed of V-velocity profiles along a horizontal line passing through the geometric centre of the cavity (at Y= 0.5) at various aspect ratios, Re = 1000.

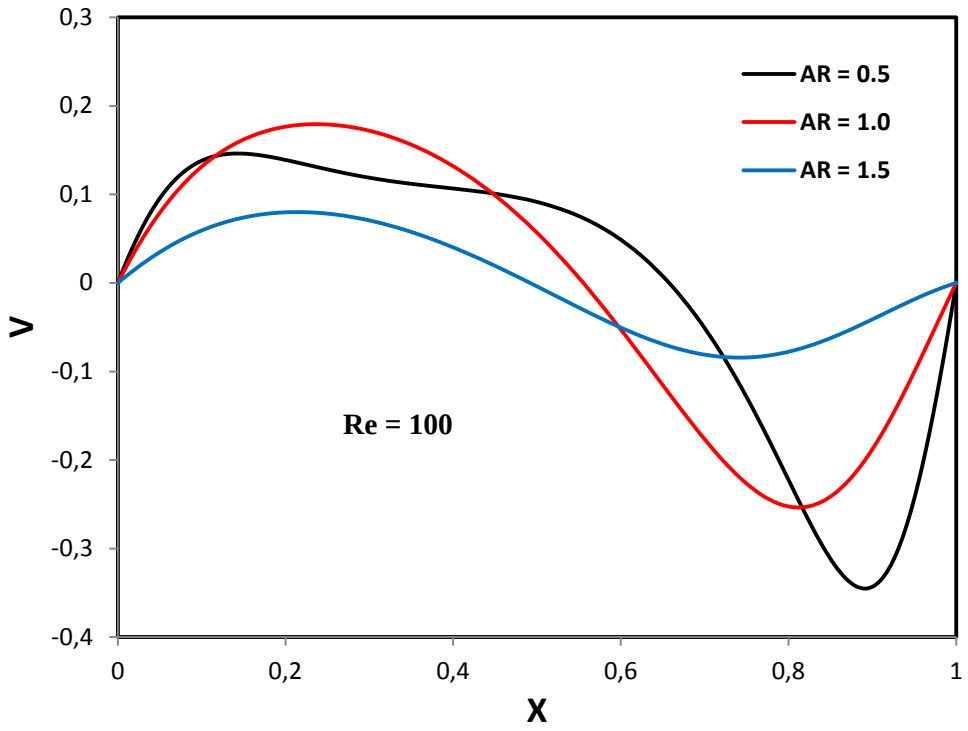

Figure 7: Computed of V-velocity profiles along a horizontal line passing through the geometric centre of the cavity (at Y= 0.5) at various aspect ratios, Re = 100.

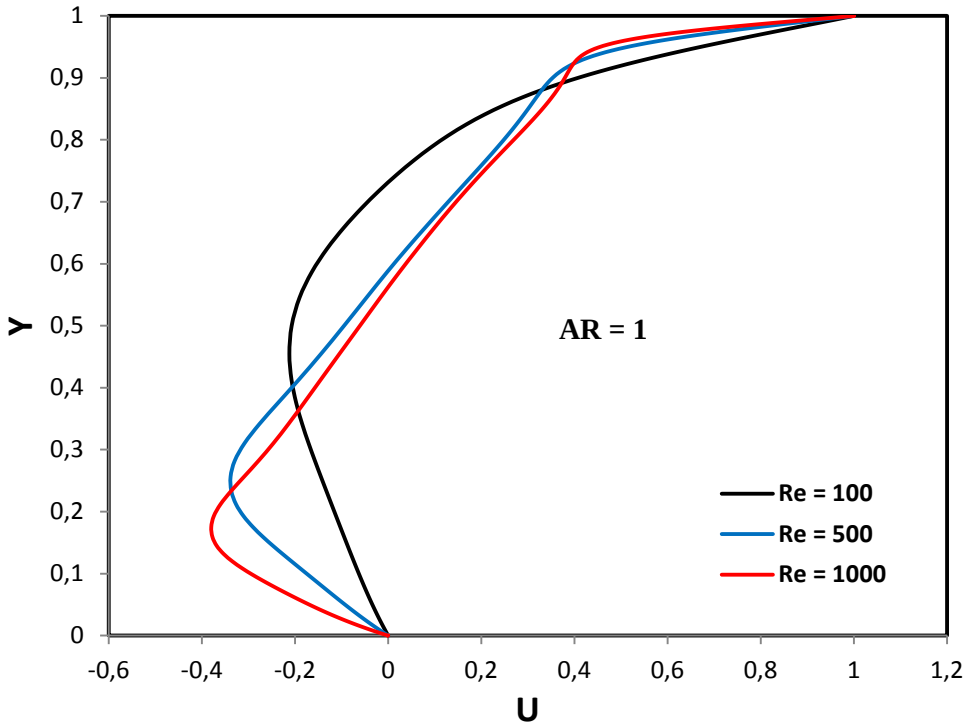

Figure 8: Computed of U-velocity profiles along a vertical line passing through the geometric centre of the cavity (at X= 0.5) at various Reynolds number, AR = 1.

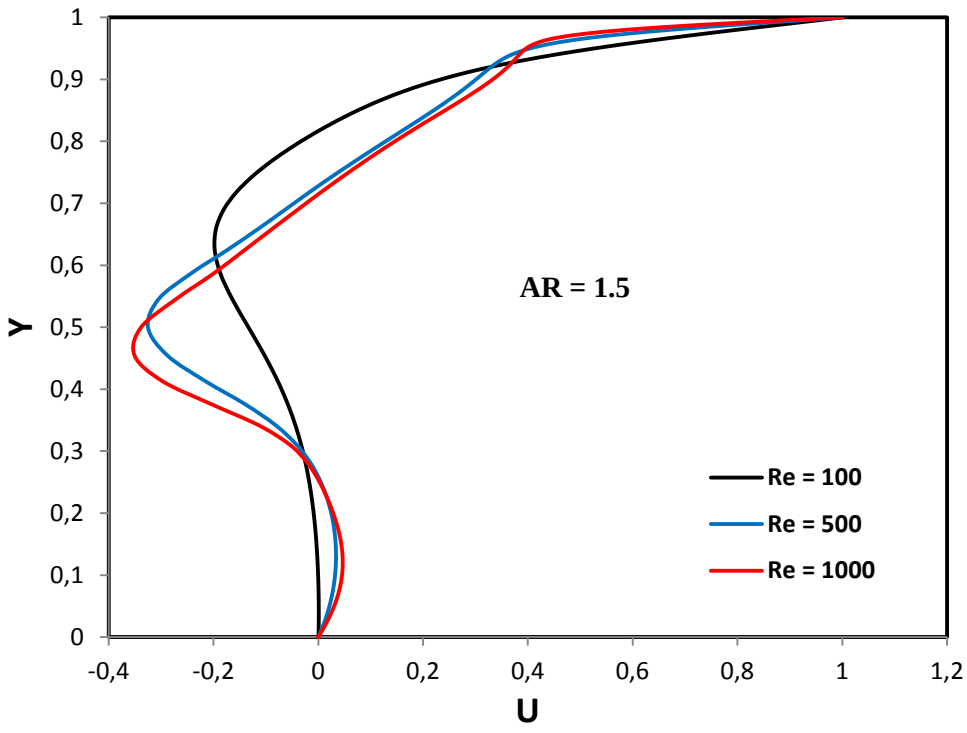

Figure 9: Computed of U-velocity profiles along a vertical line passing through the geometric centre of the cavity (at X= 0.5) at various Reynolds number, AR = 1.5.

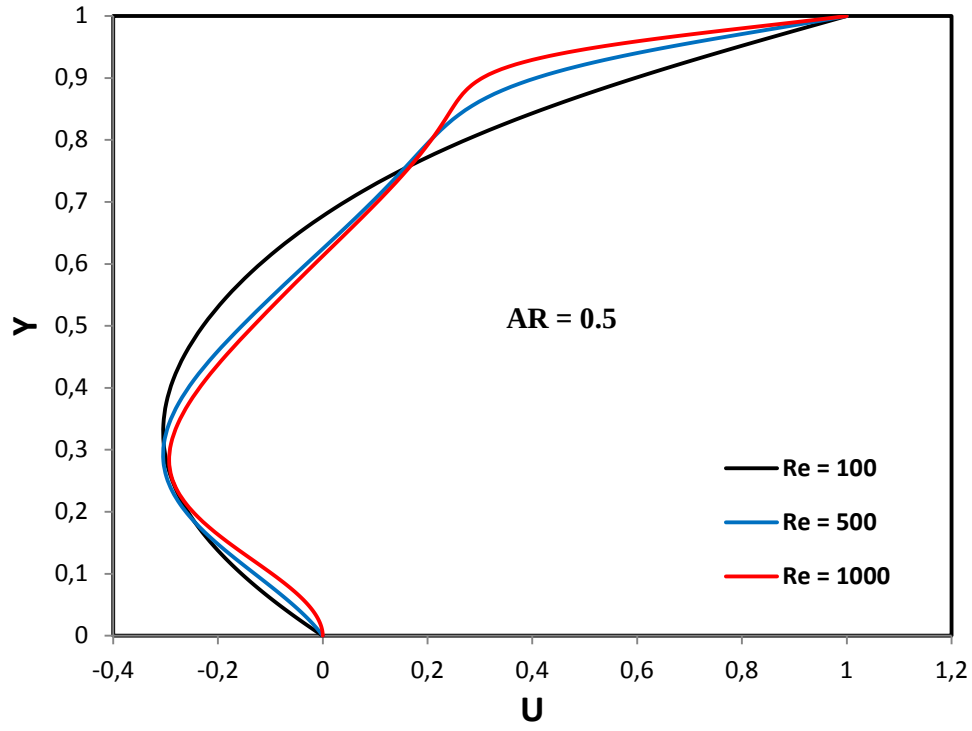

Figure 10: Computed of U-velocity profiles along a vertical line passing through the geometric centre of the cavity (at X= 0.5) at various Reynolds number, AR = 0.5.

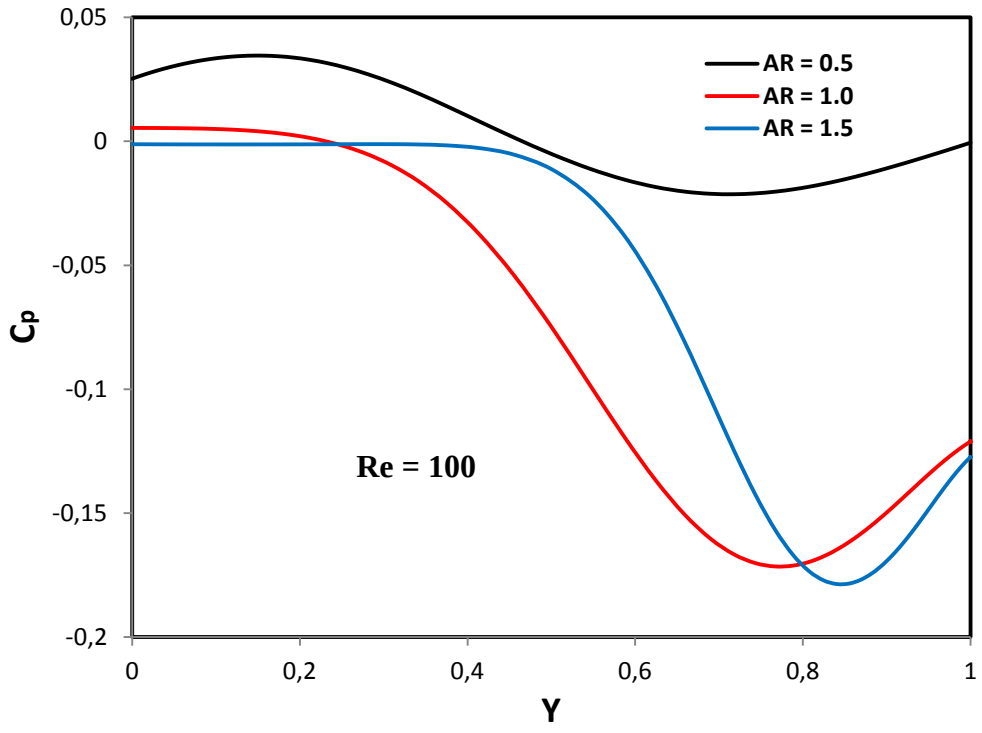

Figure 11: Computed of pressure coefficient along a vertical line passing through the geometric centre of the cavity (at X= 0.5) at various aspect ratios, Re = 100.

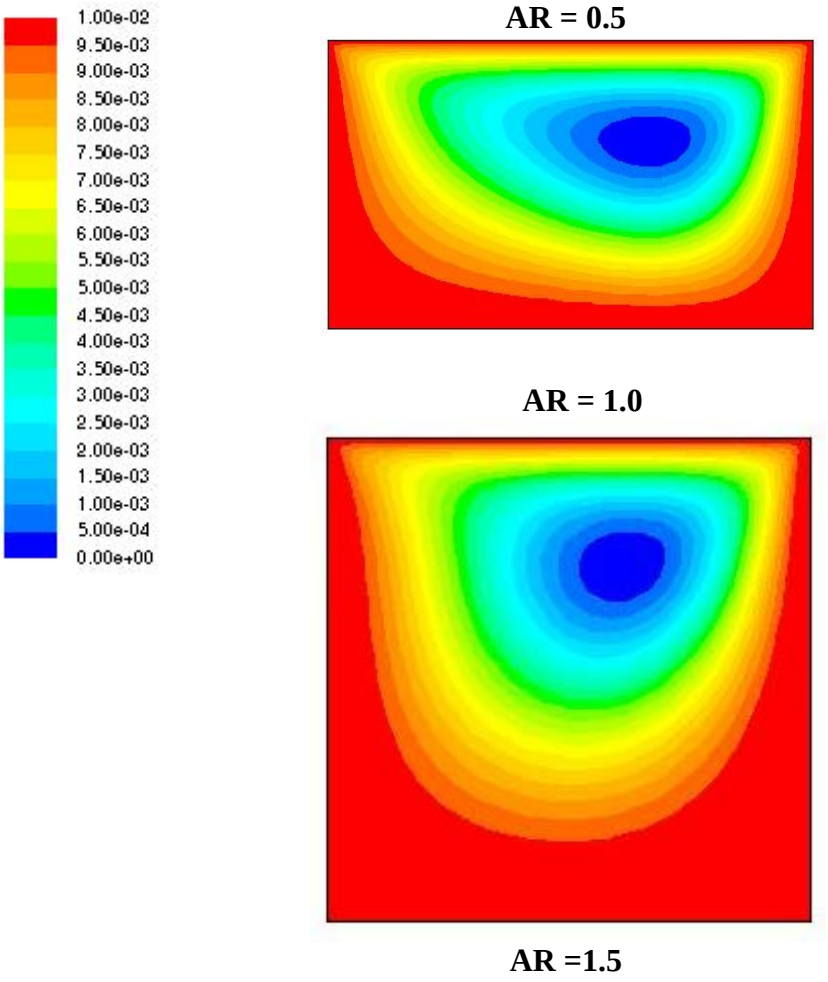

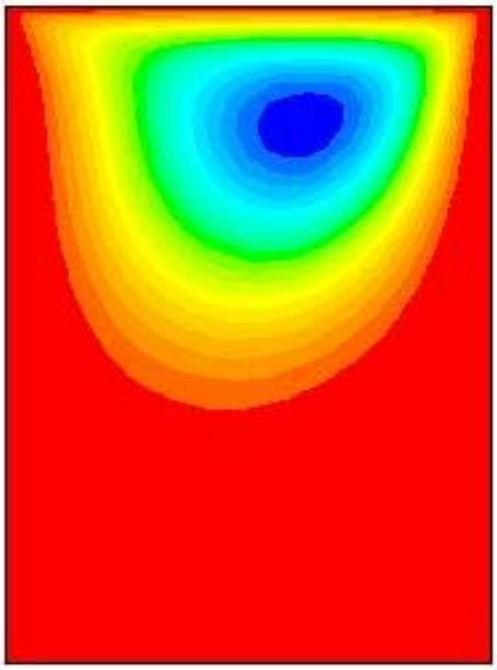

Figure 12: Contours of stream function at different aspect ratio for *R*e = 100.

AR = 0.5

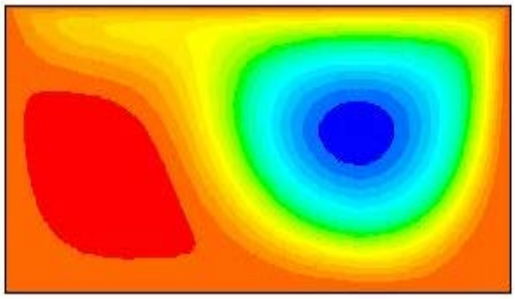

AR = 1.0

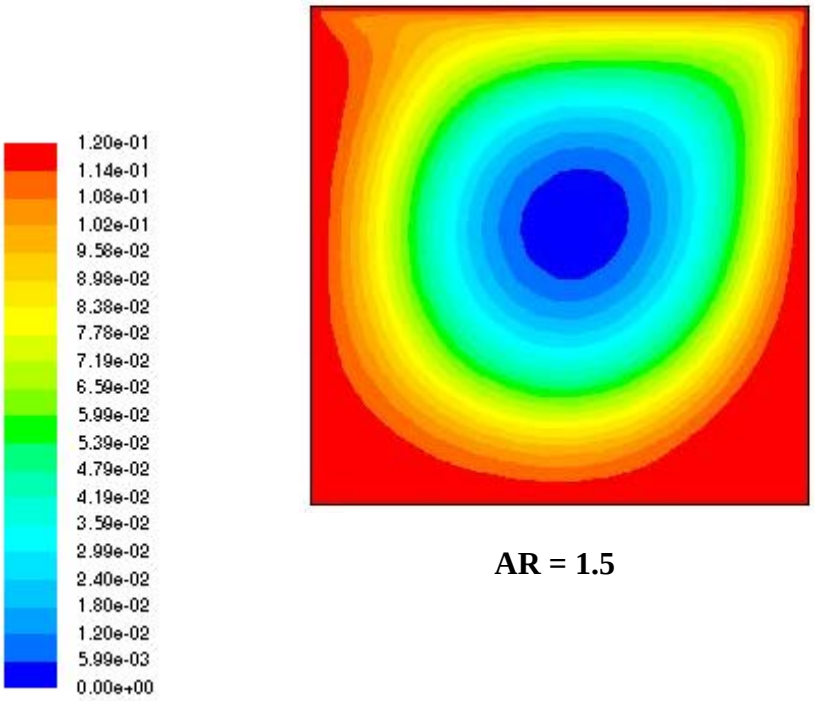

AR = 1.5

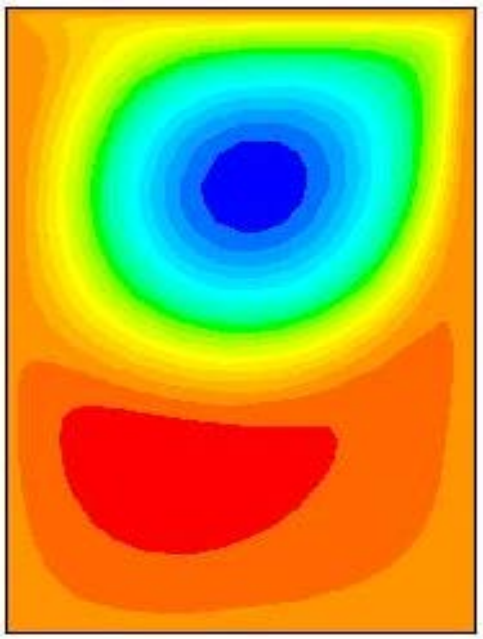

Figure 13: Contours of stream function at different aspect ratio for *R*e = 1000.

Nomenclature

L	[m]	length of the cavity in the flow direction
H	[m]	height of the cavity in the direction normal to the flow
AR	[-]	aspect ratio *H/L*
C_p	[-]	pressure drag coefficient
P	[N/m^2]	pressure
*R*e	[-]	Reynolds number
U_∞	[m/s]	lid velocity
U	[m/s]	x-component velocity
V	[m/s]	y-component velocity

Greek Symbols

μ	[Pa.s]	fluid dynamic viscosity
ρ	[kg/m^3]	fluid density